



Cite this: *Chem. Commun.*, 2015, 51, 16988

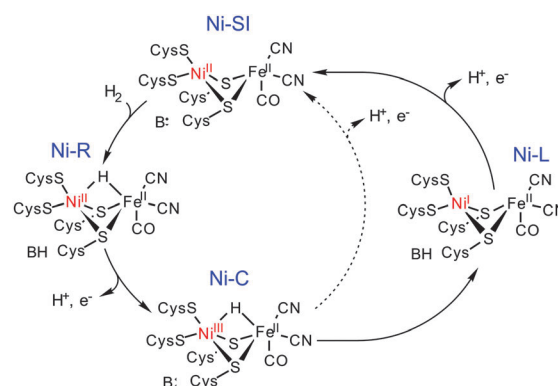
Received 15th July 2015,  
Accepted 30th September 2015

DOI: 10.1039/c5cc05881c

www.rsc.org/chemcomm

**[Ni(L<sup>I</sup>)Fe(‘BuNC)<sub>4</sub>](PF<sub>6</sub>)<sub>2</sub> is a robust Ni<sup>I</sup>Fe<sup>II</sup> complex that undergoes a reversible one-electron reduction. Spectroscopic and theoretical studies show that [Ni(L<sup>I</sup>)Fe(‘BuNC)<sub>4</sub>]<sup>+</sup> is an unprecedented Ni<sup>I</sup>Fe<sup>II</sup> species that reproduces the electronic configuration of the Ni-L state of the [NiFe] hydrogenases.**

The [NiFe]-hydrogenases catalyse the two-electron inter-conversion of two protons and molecular hydrogen.<sup>1</sup> The nature of the Ni-Fe heterobimetallic active site in these enzymes is now established; the Ni centre is co-ordinated by two terminal and two bridging cysteinyl donors, which co-ordinate to a Fe centre that is also bound by one carbonyl and two cyanide ligands (Scheme 1). Catalytic H<sub>2</sub> cleavage is associated with changes in the formal oxidation state of the Ni centre while the Fe centre remains in the Fe<sup>II</sup> state during turnover.<sup>1c</sup> Three key states have been identified in a catalytic cycle (Scheme 1): Ni-SI, Ni-R and Ni-C. Thus, H<sub>2</sub> reacts with Ni-SI and undergoes heterolytic cleavage to form Ni-R which contains a bridging H<sup>-</sup> ligand. A co-ordinated Cys ligand may act as an initial proton acceptor for the accompanying proton before its transfer to other bases (B) about the active site.<sup>3</sup> The removal of an electron generates the EPR active *S* = 1/2 Ni-C state, which can be converted to an EPR-active *S* = 1/2 Ni<sup>I</sup>Fe<sup>II</sup> state (Ni-L) following the photolysis at low temperatures.<sup>4</sup> Previously, Ni-L had not been viewed as being catalytically relevant given the conditions required for its formation. However, recent *in situ* IR spectroelectrochemical studies have demonstrated that Ni-L may be generated reversibly in the dark under turnover conditions.<sup>2</sup> Therefore, the regeneration of the Ni-SI state could occur either directly from the Ni-C state, *via* the concerted transfer of an electron and a proton, or by oxidation



**Scheme 1** A proposed catalytic cycle for H<sub>2</sub> oxidation by the [NiFe] hydrogenases showing regeneration of Ni-SI directly from Ni-C (dotted line) or *via* a recently proposed route involving Ni-L (solid line).<sup>2</sup>

of the Ni-L state. These studies, together with previous DFT calculations,<sup>5</sup> open up the possibility that separate proton and electron transfer events may be associated with the regeneration of the Ni-SI state from Ni-C, and that these steps may involve the Ni-L state (Scheme 1).

Despite the large number of diamagnetic Ni<sup>I</sup>Fe<sup>II</sup> complexes that have been prepared as analogues of the [NiFe] hydrogenases,<sup>6</sup> the syntheses of paramagnetic analogues have proven to be more challenging.<sup>7</sup> Several Ni<sup>III</sup>Fe<sup>III</sup>, Ni<sup>II</sup>Fe<sup>III</sup>, Ni<sup>II</sup>Fe<sup>I</sup> and Ni<sup>I</sup>Fe<sup>I</sup> centres have been reported,<sup>6c,7,8</sup> none of which have succeeded in reproducing the crucial Ni<sup>I</sup>Fe<sup>II</sup> and Ni<sup>III</sup>Fe<sup>II</sup> states found for the [NiFe] hydrogenases. For example, [(dppe)Ni(μ-pdt)Fe(CO)<sub>3</sub>](BF<sub>4</sub>)<sup>7</sup> [dppe = 1,2-bis(diphenylphosphino)ethane, pdt = propane-1,2-dithiolate] possesses a Ni<sup>I</sup>Fe<sup>I</sup> configuration with spin density localised principally on the Fe centre and [(dppe)Ni(μ-pdt)Ru(cymene)]<sup>9</sup> possesses a Ni<sup>I</sup>Ru<sup>II</sup> centre rather than the biologically more relevant Ni<sup>I</sup>Fe<sup>II</sup> unit. Given the renewed focus on the role of Ni-L, we report the characterisation of a Ni<sup>I</sup>Fe<sup>II</sup> complex ([1]<sup>+</sup>) as an analogue of this state. [1]<sup>+</sup> is prepared from the reversible, one-electron reduction of the parent complex [1]<sup>2+</sup> (Fig. 1). Our assignment of [1]<sup>+</sup> as a Ni<sup>I</sup>Fe<sup>II</sup> centre represents the first analogue of the Ni-L form of the

<sup>a</sup> The University of Nottingham, University Park, Nottingham, NG7 2RD, UK.  
E-mail: j.mcmaster@nottingham.ac.uk

<sup>b</sup> The University of Manchester, Oxford Road, Manchester, M13 9PL, UK.  
E-mail: m.schroder@manchester.ac.uk

† Electronic supplementary information (ESI) available: Experimental and theoretical procedures, additional crystallographic, spectroscopic and electrochemical data. CCDC 1410033. For ESI and crystallographic data in CIF or other electronic format see DOI: 10.1039/c5cc05881c



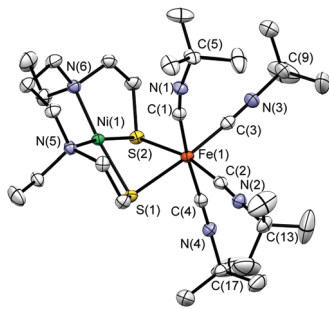


Fig. 1 X-Ray structure of the cation  $[1]^{2+}$  in  $[1](PF_6)_2$  with 50% probability thermal ellipsoids.

$[NiFe]$  hydrogenases to feature Ni and Fe centres with electronic configurations that mirror those proposed for Ni-L.

Treatment of a solution of  $[Ni(L^1)]$  ( $H_2L^1 = N,N'$ -diethyl-3,7-diazanonane-1,9-dithiol)<sup>10</sup> in acetonitrile with  $FeCl_2$  followed by the addition of four equivalents of  $tBuNC$  and  $NH_4PF_6$  affords  $[Ni(L^1)Fe(tBuNC)_4](PF_6)_2$  ( $[1](PF_6)_2$ ).  $[1](PF_6)_2$  is stable at room temperature in air as a solid and in acetonitrile solution for at least 48 h, as monitored by IR spectroscopy. The crystallographic characterisation of  $[1](PF_6)_2 \cdot MeCN$  shows the Ni centre in an approximate square-planar  $N_2S_2$  environment with Fe having a pseudo-octahedral co-ordination sphere comprised of four  $tBuNC$  ligands and two S donors derived from  $[Ni(L^1)]$  (Fig. 1). The  $NiN_2S_2$  fragment retains the structural features of the  $[Ni(L^1)]$  precursor,<sup>11</sup> the most significant difference being a smaller  $S(1)-Ni(1)-S(2)$  angle  $[81.76(2)^\circ]$  in  $[Ni(L^1)]$  relative to that in  $[1]^{2+}$   $[84.20(2)^\circ]$ . This difference may reflect the steric demands of the co-ordinated  $[Fe(tBuNC)_4]^{2+}$  fragment in  $[1]^{2+}$ . The equatorial  $tBuNC$  ligands defined by C(2) and C(3) bind to Fe(1) in an essentially linear mode with  $Fe(1)-C-N$  angles of  $175.3(2)^\circ$  and  $175.1(2)^\circ$ , respectively. In contrast the axial  $tBuNC$  ligands, defined by C(1) and C(4), co-ordinate in a bent geometry with  $Fe(1)-C-N$  angles of  $170.0(2)$  and  $172.9(2)^\circ$ , respectively. The  $Ni(1)-C(1)$  and  $Ni(1)-C(4)$  distances  $[2.951(2)$  and  $4.164(2)$  Å, respectively] are significantly greater than the  $Fe(1)-C(1)$  and  $Fe(1)-C(4)$  distances  $[1.890(2)$  and  $1.888(2)$  Å, respectively]. Thus, the axial  $tBuNC$  ligands do not appear to adopt bridging modes between the Ni and Fe centres in  $[1]^{2+}$  and the non-linear binding mode of these ligands about Fe(1) may result from inter- and intra-molecular interactions due to crystal packing (Fig. S1, ESI<sup>†</sup>). The  $Ni(1)-Fe(1)$  distance  $[2.9898(7)$  Å] compares well with that in the inactive oxidised form of  $[NiFe]$  hydrogenase from *Desulfovibrio gigas* (2.9 Å)<sup>12</sup> and is significantly longer than that found in the Ni-R form from *Desulfovibrio vulgaris* Miyazaki F (2.57 Å)<sup>3a</sup> that both contain Ni and Fe in formal  $M^{II}$  oxidation states.

The cyclic voltammogram of  $[1](PF_6)_2$ , recorded at 298 K in MeCN containing 0.2 M  $[N^rBu_4][BF_4]$  as supporting electrolyte, shows a reduction process at  $E_{1/2} = -1.39$  V vs.  $Fc^+/Fc$  that is reversible over the range of scan rates employed in the experiment (20–300  $mV s^{-1}$ , Fig. S2 and S3, ESI<sup>†</sup>). The cyclic voltammogram of  $[Ni(L^1)]$  recorded under the same conditions reveals a reduction process at  $E_p^c = -2.35$  V vs.  $Fc^+/Fc$  (Fig. S4, ESI<sup>†</sup>), assigned to the reduction of  $[Ni(L^1)]$  to the formal  $Ni^I$  state on the basis of

comparisons with previously reported  $NiN_2S_2$  complexes possessing similar co-ordination spheres.<sup>13</sup> The shift of ca. +1 V for the reduction of  $[1](PF_6)_2$  relative to that of  $[Ni(L^1)]$  is consistent with the formation of a Lewis base Lewis acid adduct between  $[Ni(L^1)]$  and  $[Fe(tBuNC)_4]^{2+}$ ; ca. +0.5 V shifts in potential have been observed previously for  $(NiN_2S_2)W(CO)_4$  relative to their parent  $NiN_2S_2$  complexes.<sup>13</sup> UV/vis spectroelectrochemistry indicates that  $[1]^+$  decomposes at temperatures above 273 K and that cooling to 243 K is required to ensure the quantitative regeneration of  $[1]^{2+}$  (Fig. S5 and Table S1, ESI<sup>†</sup>). On cooling to 243 K the cyclic voltammogram of  $[1](PF_6)_2$  becomes electrochemically irreversible (Fig. S6, ESI<sup>†</sup>) and the controlled potential electrolysis of  $[1](PF_6)_2$  at  $-1.6$  V vs.  $Fc^+/Fc$  at 243 K confirms that a one-electron reduction process accompanies the formation of  $[1]^+$ . The cyclic voltammograms of  $[1](PF_6)_2$  and  $[1]^+$  at 243 K exhibit similar profiles confirming the stability of  $[1]^+$  under the conditions and timescale of the experiment (Fig. S7, ESI<sup>†</sup>).

The IR spectra of  $[1](PF_6)_2$  and  $[1]^+$  in MeCN solution are shown in Fig. 2. Each spectrum exhibits four bands assigned to the C–N stretches of the  $tBuNC$  ligands. In  $[1]^{2+}$  these bands occur at frequencies typical of isonitrile ligands bound in a terminal mode to transition metal centres.<sup>14</sup> The overall shift of the bands to lower frequencies following the reduction of  $[1]^{2+}$  to  $[1]^+$  is consistent with an increase in the electron density about the Ni–Fe core and a corresponding increase in  $\pi$ -back-donation into the  $tBuNC$  units. A C–N stretching band at  $1857$   $cm^{-1}$  in the IR spectrum of  $[1]^+$  in MeCN solution suggests that one terminal, apical  $tBuNC$  ligand moves to a bridging mode between the Ni and Fe centres (Fig. 2) following the reduction of  $[1]^{2+}$ ; a similar bridging mode is found in  $[Fe_2(pdt)(MeNC)_7](PF_6)_2$  where one MeNC ligand bridges between the two Fe centres.<sup>15</sup>

The X-band EPR spectrum of electrochemically generated  $[1]^+$  recorded at 77 K in MeCN/0.2 M  $[N^rBu_4][BF_4]$  (Fig. 3a) shows striking similarities to those of  $Ni^I N_2S_2$  complexes ( $S =$  thiolato, thioether or sulfonato,  $N =$  amine donors;  $g_{||} = 2.18-2.25$ ;  $g_{\perp} = 2.057-2.071$ ), generated by chemical reduction of their  $Ni^{II}$  counterparts,<sup>16</sup> and, crucially, is substantially different to those of  $Fe^I$  centres including  $[Fe(CO)_3(PPh_3)_2]^+$

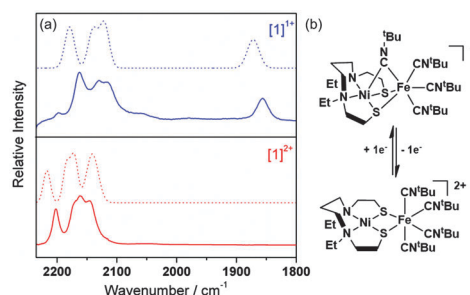
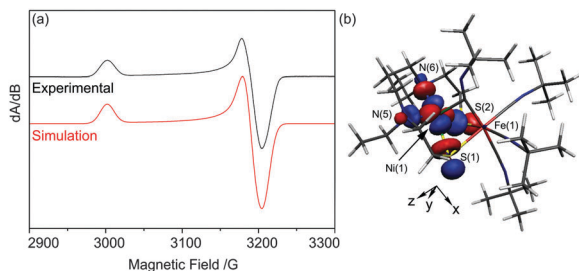


Fig. 2 (a) Solution IR spectra of  $[1](PF_6)_2$  (2200, 2170, 2161 and  $2144$   $cm^{-1}$ ) and  $[1]^+$  (2162, 2129, 2116 and  $1857$   $cm^{-1}$ ) recorded in MeCN (solid lines) and DFT calculated spectra (dotted lines; 2216, 2183, 2169,  $2139$   $cm^{-1}$  for  $[1]^{2+}$  and 2179, 2140, 2121,  $1872$  for  $[1]^+$ ). (b) Proposed rearrangement supported by DFT calculations.





**Fig. 3** (a) X-band EPR spectrum of  $[1]^+$  as a solution in MeCN/0.2 M  $[N^tBu_4][BF_4]$  at 77 K. Experimental (black) and simulated (red) spectrum, simulated using the spin Hamiltonian parameters  $g_{11} = 2.210$ ,  $g_{22} = g_{33} = 2.074$  ( $W_{11} = 18$ ,  $W_{22} = 16$ ,  $W_{33} = 17$  G); (b) the Kohn-Sham SOMO of  $[1]^+$  plotted with an isosurface value of  $0.05 e^- \text{ \AA}^{-3}$ .

( $g_{xx} = 2.053$ ,  $g_{yy} = 2.090$ ,  $g_{zz} = 2.001$ )<sup>17</sup> and  $[(dppe)Ni(\mu\text{-pdt})Fe(CO)_3]^+$  ( $g_{xx} = 2.052$ ,  $g_{yy} = 2.050$ ,  $g_{zz} = 2.005$  for one isomer).<sup>7</sup> Thus, the EPR spectroscopic data are consistent with a formal  $Ni^I Fe^II$  unit in  $[1]^+$  where the  $Ni^I$  centre adopts a  $d^9$ ,  $S = 1/2$  configuration in which the unpaired electron resides in d-orbital orientated in the equatorial plane of the  $Ni^I N_2 S_2$  unit with associated spin Hamiltonian parameters  $g_{zz} > g_{xx} \approx g_{yy} > g_e$ .<sup>18</sup> In contrast, the Ni-L form of the  $[NiFe]$  hydrogenases is characterised by a rhombic EPR spectrum ( $g_{11} = 2.30$ ,  $g_{22} = 2.12$  and  $g_{33} = 2.05$ )<sup>19</sup> that may be viewed as resulting from the re-hybridisation of the Ni  $d_{x^2-y^2}$  and  $d_{z^2}$  orbitals in Ni-C where one hybrid contributes to a Ni-Fe bond.<sup>20</sup> The UV/vis spectrum of  $[1]^+$  (Table S1 and Fig. S5, ESI<sup>†</sup>) shows bands at 400 (3900), 490 (1760), 520 (1500), 598 (1100) and 720 nm ( $380 M^{-1} cm^{-1}$ ) that are consistent with those in the UV/vis spectra of other well-defined  $Ni^I$  complexes.<sup>21</sup>

In order to support the  $Ni^I Fe^II$  assignment proposed for  $[1]^+$ , we conducted density functional theory (DFT) calculations on the full structures of  $[1]^{2+/+}$ . The calculated structure of  $[1]^{2+}$  [Fig. S8(a), ESI<sup>†</sup>] reproduces the principal features of the experimentally determined structure (Fig. 1); the average Fe-C distances are *ca.* 0.02 Å shorter and the Ni-S and Fe-S distances are *ca.* 0.04 Å longer in the calculated structure of  $[1]^{2+}$  (Table S3, ESI<sup>†</sup>). The principal differences between the calculated and experimental structures are (i) a relaxation of the dihedral angle defined by the S(1)-Ni(1)-S(2) and S(1)-Fe(1)-S(2) planes [ $117.94(3)^\circ$  and  $128.3^\circ$ , in the calculated and experimental structures, respectively], (ii) an increase in the Ni(1)-Fe(1) distance of *ca.* 0.2 Å in the calculated relative to the experimental structure of  $[1]^{2+}$  [Ni(1)-Fe(1) = 3.209 Å and 2.9896(4) Å for the calculated and experimental structures, respectively, Table S2, ESI<sup>†</sup>], and (iii) an increase in the C-Fe(1)-C and Fe(1)-C-N angles for the axial <sup>t</sup>BuNC ligands defined by C(1) and C(4) (Table S2, ESI<sup>†</sup>). The unscaled<sup>22</sup> calculated IR spectrum of  $[1]^{2+}$  possesses four bands in the C-N stretching region at 2216, 2183, 2169 and 2139  $cm^{-1}$  that compare well with the experimental stretching frequencies (Fig. 2). Thus, the close correspondence between the calculated and experimental structures, and IR spectra suggest that the DFT calculations provide a reasonable description of the geometric and electronic structure of  $[1]^{2+}$ . The composition<sup>23</sup> of the HOMO in  $[1]^{2+}$

shows that it is largely metal-centred [59.3% Ni  $d_{z^2}$ , 0.6% Ni  $d_{xz}$ , 9.7% Fe  $d_{x^2-y^2}$ , 1.2% Fe  $d_{xz}$ , S 25.8%, N(5) + N(6) 1.2%, Fig. S9, ESI<sup>†</sup>]. The Mayer bond order<sup>24</sup> between the Ni(1) and Fe(1) centres (0.04) derived from the DFT calculations suggests there is no formal metal-metal bond in  $[1]^{2+}$ . Overall the description of the electronic structure of  $[1]^{2+}$  is consistent with an  $S = 0$   $Ni^II Fe^II$  centre in  $[1]^{2+}$ .

The calculated structure of  $[1]^+$  suggests that significant changes in geometry about the Ni(1) and Fe(1) centres accompany the reduction of  $[1]^{2+}$  [Fig. S8(b) and Table S3, ESI<sup>†</sup>]. These include a marked decrease in the dihedral angle between the S(1)-Ni(1)-S(2) and S(1)-Fe(1)-S(2) planes ( $94.1^\circ$  and  $128.3^\circ$ , for  $[1]^+$  and  $[1]^{2+}$ , respectively) and a shortening of the Ni(1)-Fe(1) distance [Ni(1)-Fe(1) = 2.616 Å and 3.209 Å for  $[1]^{1+}$  and  $[1]^{2+}$ , respectively], which compares well with that calculated for models of the active site of the Ni-L form.<sup>20</sup> On the reduction of  $[1]^{2+}$  one axial <sup>t</sup>BuNC ligand, defined by C(1), moves to a bridging mode between the Fe(1) and Ni(1) centres with Fe(1)-C(1) and Ni(1)-C(1) distances of 1.942 and 2.018 Å, respectively. The adoption of a bridging mode for this ligand is accompanied by a significant bend in the backbone of the ligand [C(1)-N(1)-C(5) =  $140.9^\circ$ ], which is commonly observed for bridging isocyanides.<sup>25</sup> The calculated IR spectrum for  $[1]^+$  shows three intense C-N stretches at 2179, 2140 and 2121  $cm^{-1}$  for the terminal isocyanides and a single band at 1872  $cm^{-1}$  for the C-N stretching mode of the bridging <sup>t</sup>BuNC ligand. This calculated spectrum shows close correspondence to the experimental IR spectrum of  $[1]^+$  (Fig. 2) and strongly supports a structural rearrangement in which a terminal <sup>t</sup>BuNC ligand moves to a bridging mode on the reduction of  $[1]^{2+}$ . This structural rearrangement may also underpin the differences in profiles of the cyclic voltammograms of  $[1](PF_6)_2$  recorded at 298 K (Fig. S2, ESI<sup>†</sup>) and 243 K (Fig. S6, ESI<sup>†</sup>). The rate of the suggested structural rearrangements for  $[1]^{2+/+}$  may be slowed at 243 K with the consequent loss of electrochemical reversibility for the  $[1]^{2+/+}$  process at 243 K. We are unable to determine the precise mechanism that gives rise to the voltammetric profile *i.e.* whether electron transfer precedes structural rearrangement or *vice versa*. However, the results of the UV/vis spectroelectrochemical experiments clearly show that the process is chemically reversible at 243 K over the timescale of this experiment.

The SOMO of  $[1]^+$  possesses 60.8% Ni  $d_{xy}$ , 1.3% Ni  $d_{xz}$ , 1.1% Ni  $d_{yz}$ , S 21.7%, N(5) + N(6) 10.2% character and is essentially localised on the  $NiN_2S_2$  unit (Fig. 3b). The calculated EPR spin Hamiltonian parameters using the BP86 functional ( $g_{zz} = 2.174$ ,  $g_{yy} = 2.079$ ,  $g_{xx} = 2.070$ , Table S2, ESI<sup>†</sup>) reproduce the approximately axial nature of the frozen solution EPR spectrum of  $[1]^+$  (Fig. 3a). We note that the DFT calculations underestimate the largest *g*-shift ( $g_{zz} = 2.174$  calc. vs.  $g_{11} = 2.210$ ). Such underestimations (by up to 30%) have been observed previously for various metal centres including  $Ni^I$ , and these underestimations have been attributed partly to overestimations in spin delocalisation into ligand-based orbitals in the calculated electronic structures.<sup>20,26</sup> Thus, these results, together with the excellent agreement between the calculated and experimental IR spectra,



support a  $\text{Ni}^{\text{I}}\text{Fe}^{\text{II}}$  description for  $[\mathbf{1}]^+$  where the unpaired electron is essentially localised in the  $d_{xy}$  orbital of a  $d^9$   $\text{Ni}^{\text{I}}$  centre. The calculated Ni–Fe Mayer bond order increases from 0.04 in  $[\mathbf{1}]^{2+}$  to 0.20 in  $[\mathbf{1}]^+$  indicating the development of a Ni–Fe interaction but not a direct bond. In contrast, DFT calculations on models of the Ni–L state possess Ni–Fe bond orders of *ca.* 0.40 supporting the formation of a metal–metal bond in these centres.<sup>20</sup> The absence of a formal Ni–Fe bond in  $[\mathbf{1}]^+$  is not surprising given the additional fourth  $\text{tBuNC}$  ligand in the co-ordination sphere of  $\text{Fe}^{\text{II}}$  which occupies a bridging position between the Ni and Fe centres; this site is vacant in structures proposed for Ni–L.

Ni–L reacts with CO and converts to the paramagnetic Ni–CO state which features a CO ligand bound to the  $\text{Ni}^{\text{I}}$  centre.<sup>27</sup> Thus, we examined the reactivity of  $[\mathbf{1}]^{2+}$  and  $[\mathbf{1}]^+$  towards CO. Whereas  $[\mathbf{1}]^{2+}$  does not react with CO, a solution of  $[\mathbf{1}]^{1+}$  chemically generated from  $[\mathbf{1}](\text{PF}_6)$  with  $[\text{Cp}^*\text{Co}]$  readily reacts with CO at 243 K, as monitored by IR spectroscopy (Fig. S10, ESI<sup>†</sup>). Several new bands develop in the C–O and C–N stretching region and the frozen solution EPR spectrum exhibits multiple low field features (Fig. S10, ESI<sup>†</sup>) suggesting the formation of multiple products, which proved intractable.

In conclusion,  $[\mathbf{1}]^{2+}$  has been prepared and structurally characterised as its  $[\mathbf{1}](\text{PF}_6)_2$  salt. The electrochemical one-electron reduction of  $[\mathbf{1}]^{2+}$  generates paramagnetic  $[\mathbf{1}]^+$  which has been characterized by IR, UV/vis and EPR spectroscopies. DFT calculations reproduce the principal features of the IR spectrum of  $[\mathbf{1}]^+$  and, in contrast to Ni–L,  $[\mathbf{1}]^+$  does not contain a formal Ni–Fe bond. Rather the formation of  $[\mathbf{1}]^+$  may be associated with a structural rearrangement that incorporates a bridging  $\text{tBuNC}$  ligand between the Ni and Fe centres. The frozen solution X-band EPR spectrum of  $[\mathbf{1}]^+$  and DFT calculated spin Hamiltonian parameters are consistent with a SOMO that is largely localized at the  $\text{NiN}_2\text{S}_2$  core in a  $\text{Ni } d_{xy}$  orbital. Thus, the experimental and theoretical data supports the assignment of  $[\mathbf{1}]^+$  to a mixed-valence  $\text{Ni}^{\text{I}}\text{Fe}^{\text{II}}$  state. In this respect  $[\mathbf{1}]^+$  represents the first example of an Ni–Fe analogue of the active site of the  $[\text{NiFe}]$  hydrogenases that reproduces the formal oxidation and spin states of the metal centres in the Ni–L form.

We thank EPSRC and the University of Nottingham for support. MS gratefully acknowledges receipt of an ERC advanced grant.

## Notes and references

- (a) J. C. Fontecilla-Camps, A. Volbeda, C. Cavazza and Y. Nicolet, *Chem. Rev.*, 2007, **107**, 4273–4303; (b) W. Lubitz, H. Ogata, O. Rüdiger and E. Reijerse, *Chem. Rev.*, 2014, **114**, 4081–4148; (c) H. Ogata, W. Lubitz and Y. Higuchi, *Dalton Trans.*, 2009, 7577–7587; (d) A. Volbeda and J. C. Fontecilla-Camps, *Dalton Trans.*, 2003, 4030–4038.
- R. Hidalgo, P. A. Ash, A. J. Healy and K. A. Vincent, *Angew. Chem., Int. Ed.*, 2015, **54**, 7110–7113.
- (a) H. Ogata, K. Nishikawa and W. Lubitz, *Nature*, 2015, **520**, 571–574; (b) A. Abou-Hamdan, P. Ceccaldi, H. Lebrette, O. Gutierrez-Sanz, P. Richaud, L. Cournac, B. Guigliarelli, A. L. De Lacey, C. Leger, A. Volbeda, B. Burlat and S. Dementin, *J. Biol. Chem.*, 2015, **290**, 8550–8558.
- (a) M. Brecht, M. van Gastel, T. Buhrke, B. Friedrich and W. Lubitz, *J. Am. Chem. Soc.*, 2003, **125**, 13075–13083; (b) J. P. Whitehead, R. J. Gurbel, C. Bagyinka, B. M. Hoffman and M. J. Maroney, *J. Am. Chem. Soc.*, 1993, **115**, 5629–5635.
- (a) S. Q. Niu, L. M. Thomson and M. B. Hall, *J. Am. Chem. Soc.*, 1999, **121**, 4000–4007; (b) A. Pardo, A. L. De Lacey, V. M. Fernandez, H. J. Fan, Y. B. Fan and M. B. Hall, *J. Biol. Inorg. Chem.*, 2006, **11**, 286–306.
- (a) S. Canaguier, V. Artero and M. Fontecave, *Dalton Trans.*, 2008, 315–325; (b) J. Dawson, C. Perotto, J. McMaster and M. Schröder, in *Bioinspired Catalysis*, ed. W. Weigand and P. Schollhammer, Wiley-VCH Verlag GmbH & Co., 2014, pp. 79–104; (c) C. Tard and C. J. Pickett, *Chem. Rev.*, 2009, **109**, 2245–2274; (d) P. A. Summers, J. Dawson, F. Ghiotto, M. W. D. Hanson-Heine, K. Q. Vuong, E. S. Davies, X.-Z. Sun, N. A. Besley, J. McMaster, M. W. George and M. Schröder, *Inorg. Chem.*, 2014, **53**, 4430–4439; (e) M. L. Helm, M. P. Stewart, R. M. Bullock, M. R. DuBois and D. L. DuBois, *Science*, 2011, **333**, 863–866; (f) C. H. Lai, J. H. Reibenspies and M. Y. Darensbourg, *Angew. Chem., Int. Ed.*, 1996, **35**, 2390–2393; (g) S. Ogo, K. Ichikawa, T. Kishima, T. Matsumoto, H. Nakai, K. Kusaka and T. Ohhara, *Science*, 2013, **339**, 682–684; (h) K. Weber, T. Kraemer, H. S. Shafaat, T. Weyhermueller, E. Bill, M. van Gastel, F. Neese and W. Lubitz, *J. Am. Chem. Soc.*, 2012, **134**, 20745–20755; (i) C. Wombwell and E. Reisner, *Chem. – Eur. J.*, 2015, **21**, 8096–8104.
- D. Schilter, M. J. Nilges, M. Chakrabarti, P. A. Lindahl, T. B. Rauchfuss and M. Stein, *Inorg. Chem.*, 2012, **51**, 2338–2348.
- (a) D. Schilter, T. B. Rauchfuss and M. Stein, *Inorg. Chem.*, 2012, **51**, 8931–8941; (b) G. Steinfeld and B. Kersting, *Chem. Commun.*, 2000, 205–206; (c) W. F. Zhu, A. C. Marr, Q. Wang, F. Neese, D. J. E. Spencer, A. J. Blake, P. A. Cooke, C. Wilson, M. Schröder and M. Schröder, *Proc. Natl. Acad. Sci. U. S. A.*, 2005, **102**, 18280–18285.
- G. M. Chambers, J. Mitra, T. B. Rauchfuss and M. Stein, *Inorg. Chem.*, 2014, **53**, 4243–4249.
- (a) F. Osterloh, W. Saak and S. Pohl, *J. Am. Chem. Soc.*, 1997, **119**, 5648–5656; (b) J. A. Denny and M. Y. Darensbourg, *Chem. Rev.*, 2015, **115**, 5248–5273.
- J. Schneider, R. Hauptmann, F. Osterloh and G. Henkel, *Acta Crystallogr., Sect. C: Cryst. Struct. Commun.*, 1999, **55**, 328–330.
- A. Volbeda, E. Garcin, C. Piras, A. L. De Lacey, V. M. Fernandez, E. C. Hatchikian, M. Frey and J. C. Fontecilla-Camps, *J. Am. Chem. Soc.*, 1996, **118**, 12989–12996.
- M. V. Rampersad, S. P. Jeffery, M. L. Golden, J. Lee, J. H. Reibenspies, D. J. Darensbourg and M. Y. Darensbourg, *J. Am. Chem. Soc.*, 2005, **127**, 17323–17334.
- R. Taylor and W. Horrocks, *Inorg. Chem.*, 1964, **3**, 584–589.
- J. D. Lawrence, T. B. Rauchfuss and S. R. Wilson, *Inorg. Chem.*, 2002, **41**, 6193–6195.
- P. J. Farmer, J. H. Reibenspies, P. A. Lindahl and M. Y. Darensbourg, *J. Am. Chem. Soc.*, 1993, **115**, 4665–4674.
- J. H. Macneil, A. C. Chiverton, S. Fortier, M. C. Baird, R. C. Hynes, A. J. Williams, K. F. Preston and T. Ziegler, *J. Am. Chem. Soc.*, 1991, **113**, 9834–9842.
- (a) A. Lappin and A. McAuley, *Adv. Inorg. Chem.*, 1988, **32**, 241–295; (b) G. Musie, P. J. Farmer, T. Tuntulani, J. H. Reibenspies and M. Y. Darensbourg, *Inorg. Chem.*, 1996, **35**, 2176–2183.
- S. Foerster, M. Stein, M. Brecht, H. Ogata, Y. Higuchi and W. Lubitz, *J. Am. Chem. Soc.*, 2003, **125**, 83–93.
- M. Kampa, M.-E. Pandelia, W. Lubitz, M. van Gastel and F. Neese, *J. Am. Chem. Soc.*, 2013, **135**, 3915–3925.
- (a) L. Gomes, E. Pereira and B. de Castro, *J. Chem. Soc., Dalton Trans.*, 2000, 1373–1379; (b) E. Pereira, L. Gomes and B. de Castro, *J. Chem. Soc., Dalton Trans.*, 1998, 629–636; (c) D. J. Szalda, E. Fujita, R. Sanzenbacher, H. Paulus and H. Elias, *Inorg. Chem.*, 1994, **33**, 5855–5863.
- J. P. Merrick, D. Moran and L. Radom, *J. Phys. Chem. A*, 2007, **111**, 11683–11700.
- A. Reed, R. Weinstock and F. Weinhold, *J. Chem. Phys.*, 1985, **83**, 735–746.
- I. Mayer, *Chem. Phys. Lett.*, 1987, **97**, 270–274.
- R. D. Adams and F. A. Cotton, *Inorg. Chem.*, 1974, **13**, 249–253.
- F. Neese, *J. Chem. Phys.*, 2003, **118**, 3939–3948.
- M.-E. Pandelia, H. Ogata, L. J. Currell, M. Flores and W. Lubitz, *Biochim. Biophys. Acta, Bioenerg.*, 2010, **1797**, 304–313.

